structure was more efficient at transferring energy to a mode two structure at SWA than to a mode one (Figure 1. 47b).

Except for the P6 interval, the baroclinic response was well described by the Wedderburn Number and the applied wind stress. The isotherms and average densities changed in the appropriate direction relative to changes in $W_N$; the isotherm tilt relaxed when $W_N$ increased from previous values and the tilt increased when $W_N$ decreased from previous values. While $W_N$ is a scalar number, baroclinic adjustments can be correctly inferred from relative changes in $W_N$. Because the observed baroclinic adjustments were well defined by the Wedderburn Number and wind stress, the internal seiche behaves as a forced system; the persistent winds did not allow the internal seiche to freely oscillate.

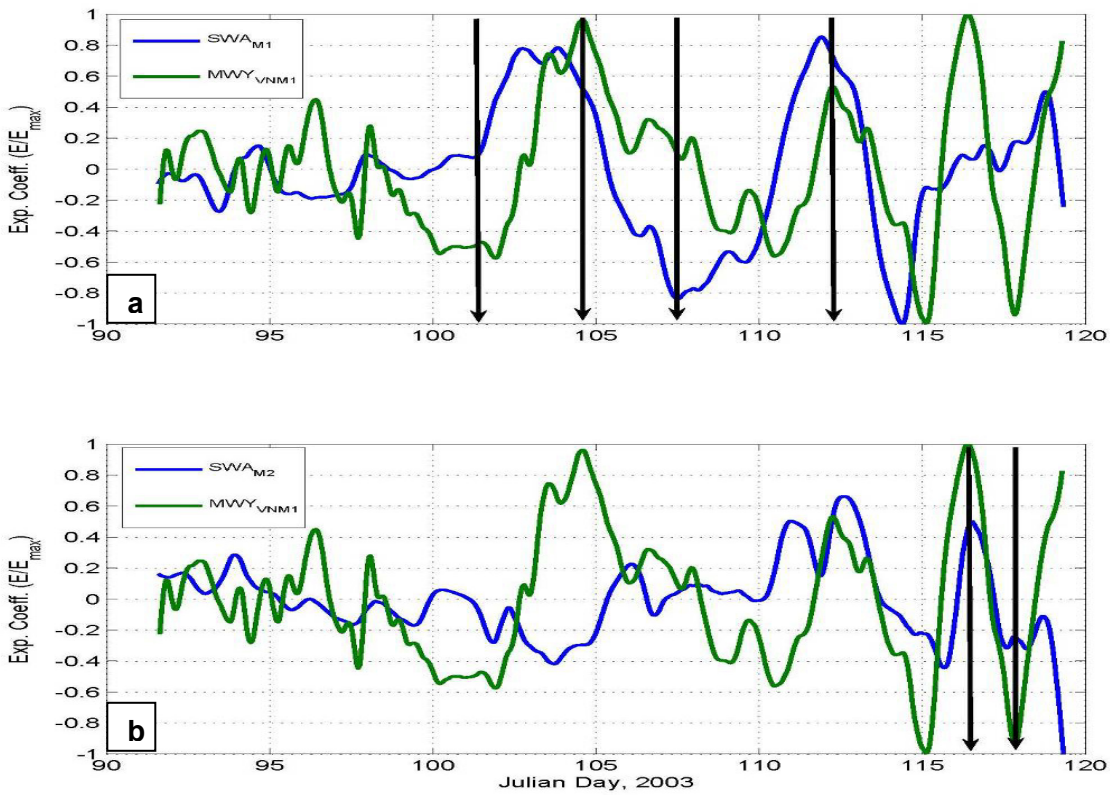


**Figure 1. 47.** Normalized mode one expansion coefficients for SWA temperature (blue) and MWY north-south velocity (green) (a) and SWA mode two temperature with MWY mode one north-south velocity (b). Vertical lines assist in showing phase relations between temperature and velocity.

1.3.3.2 2003 Observations between Temperature and Horizontal Velocity

For a freely oscillating internal seiche, temperature and velocity perturbations will be $90^o$ out-of-phase. Under wind-forced oscillations, temperature and velocity perturbations will be more in phase as velocities are affected more by wind than free wave oscillations. For example, starting with a static two-layer lake and applying a wind force on the water surface, the water will accelerate and start piling up at the downwind end. As the water piles up at the downwind end, the thermocline will depress at this end and lift at the upwind end. Thus, the velocity and temperature variance increase simultaneously with a positive correlation at the upwind end and negative at the downwind end.

This in-phase condition was observed between the mode one temperature and horizontal velocity expansion coefficients. At the arrow near JD 101, temperature and velocity increased together, but by the second arrow temperature and velocity were out-of-phase by about $45^o$ (Figure 1. 47a). At the third arrow near JD 107 to about JD 110.5, temperature and velocity are out-of-phase about $90^o$, but they are nearly in-phase by the fourth arrow near JD 112 (Figure 1. 47a). After JD 115, the second mode temperature is in-phase with the first mode horizontal velocity (Figure 1. 47b). The second mode response occurred when the wind changed directions $180^o$ three times in five days (Figure 1. 46a). The close in-phase behavior suggests the velocity and temperature responses are a forced condition and not a freely oscillating condition.

1.3.3.3 2004 Observations for Wedderburn and Lake Number, Temperature, and Wind Stress

As in the analysis of the 2003 observations, relative changes in the Wedderburn Number were compared against surface wind stress, and average density was investigated to assess relations between surface wind stress and baroclinic adjustments or isotherm tilt. Relative differences from a unit value were reviewed because $W_N$=1 indicates a balance between surface wind stress and baroclinic pressure for the conceptual model.

The Wedderburn and Lake Numbers were of comparable value with the two being nearly identical the first 20 days, after which the Lake Number diverged and became larger than the Wedderburn Number, though always by less than a factor of two (Figure 1. 48). Both number are small (<10); large-scale tilting is expected for values less than one and small to medium amplitude tilting or seiching is expected for values greater than one (Table 1. 5). The 2004 values are very similar to the values observed in 2003 (Figure 1. 45), and as for 2003 the Wedderburn Number will be used for assessing relations between surface wind stress and baroclinic adjustments.

In 2004, seven intervals were identified where $W_N$ was above or below one, and an additional interval was included in which $W_N$ was less than one but the wind switched directions 180$^o$. During Intervals P1, P3, P4, and P5, $W_N$ was less than one and between P4 and P5 the wind switched direction 180$^o$. In intervals P2, P6, and P8, $W_N$ was greater than one with $W_N$ near one in P7 (Figure 1. 49).

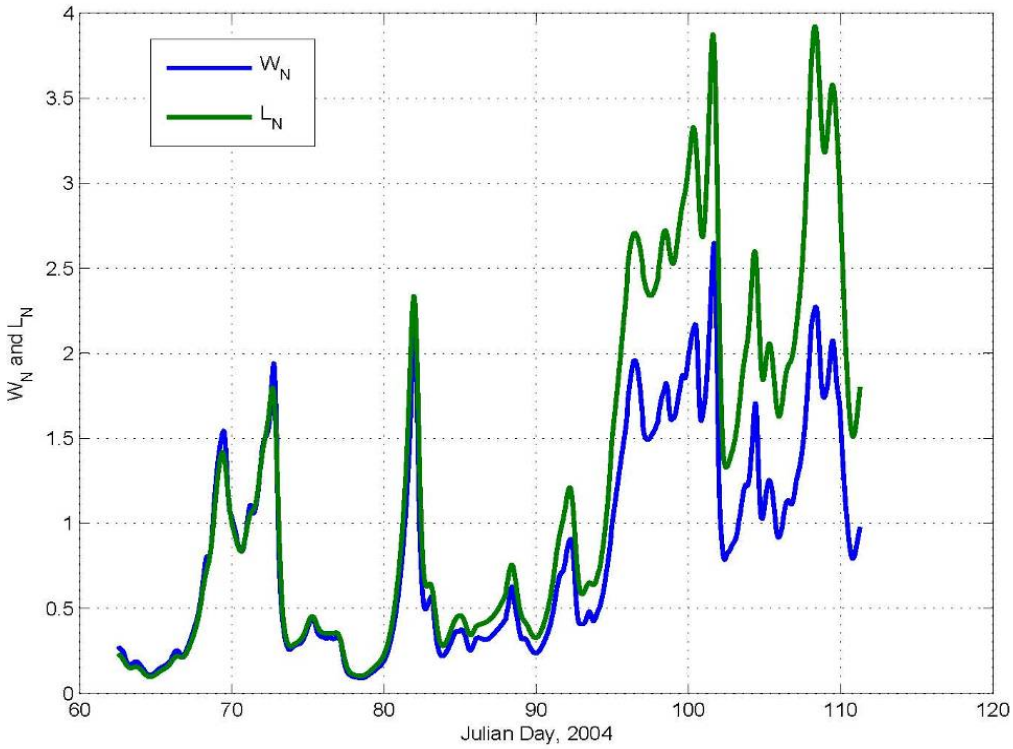


**Figure 1. 48.** Calculated Wedderburn (blue) and Lake (green) Numbers for year 2004.

During most of P1, the $W_N$ was less than 0.5 and the expansion coefficients remained fairly constant. For $W_N$ and $L_N$ less than 0.5, surface wind stress should cause significant titling of the isotherms (Table 1. 5). Significant tilting was observed below the 10-meter depth (Figure 1. 33 - Figure 1. 35). The expected V1H1 period was between 20 and 15 days and wind events were about 1.5 days apart (Figure 1. 49). Linear theory suggests the isotherms should adjust to the neutral position in 3.7 days (15/4). Because the wind events occurred more frequently, the isotherm tilt had insufficient time to relax to the neutral position. During this interval, the average density at SWA was greater than at NOA (Figure 1. 23) and the 7.3 $^{o}$C isotherm was near 10 meters at SWA and near 25 meters at NOA (Figure 1. 27).

During P2 $W_N$ was greater than during P1 because wind stress decreased, $W_N$ exceeded one, and expansion coefficients increased (temperature warmed) at SWA and decreased (temperature cooled) at NOA (Figure 1. 49). The decrease in wind stress allowed the isotherm tilt to relax, but a slight tilt was still present near JD 73; the 7.5$^{o}$C isotherm dropped to 15 meters while it was near 20 meters at NOA (Figure 1. 49). Near JD 73, the average density was nearly the same for all three locations (Figure 1. 23).

During P3 $W_N$ was less than that during P2 because the northward wind stress increased, which caused $W_N$ to decrease below 0.5. (Figure 1. 49) and significant isotherm adjustment were observed. Expansion coefficients decreased (cooled) at SWA and increased (warmed) at NOA and the SWA and NOA average densities diverged from each other (Figure 1. 49 and Figure 1. 23). Significant isotherm tilting occurred on JD 75.5 (Figure 1. 36) and near JD 78 the 7.5$^{o}$C isotherm upwelled at SWA (Figure 1. 27). The north-to-south upward tilt continued to about JD 79, when the wind stress switched to a southward direction (Figure 1. 49) and the average densities converged. However, a slight tilt was still present near JD 82 where the 7.5$^{o}$C isotherm was near 20 meters at SWA and below 25 meters at NOA (Figure 1. 23 and Figure 1. 27); this condition may be from a mode two vertical wave based on the divergent character of the 7.95 $^{o}$C and 8.16$^{o}$C isotherms. At the end of P3 $W_N$ increased above one but the duration was too short to allow a significant baroclinic adjustment; the expected adjustment time was about 2.7 days (11/4) and the event was about a day (Figure 1. 49).

During P4 $W_N$ was less than 0.5 because the northward wind stress increased, which created a persistent isotherm tilt. At the start, $W_N$ decreased and the NOA and SWA densities diverged, which corresponded to increasing expansion coefficients (warming) at NOA and decreasing expansion coefficients (cooling) at SWA (Figure 1. 49 and Figure 1. 23). During most of P4 the 7.8 $^{o}$C isotherm tilted upward from north to south: it was in the upper 10 meters at SWA, below 26 meters at NOA, and upwelled near JD 85 at SWA (Figure 1. 27). On JD 89.5 near the end of P4, the 8.3 $^{o}$C isotherm surfaced at SWA and was near 34 meters at NOA (Figure 1. 38). The expected V1H1 period was from 11 to 8 days and wind events were 1.5 days apart; intervals between wind events were smaller than density adjustment time scale of 2.3 days (9.5/4).

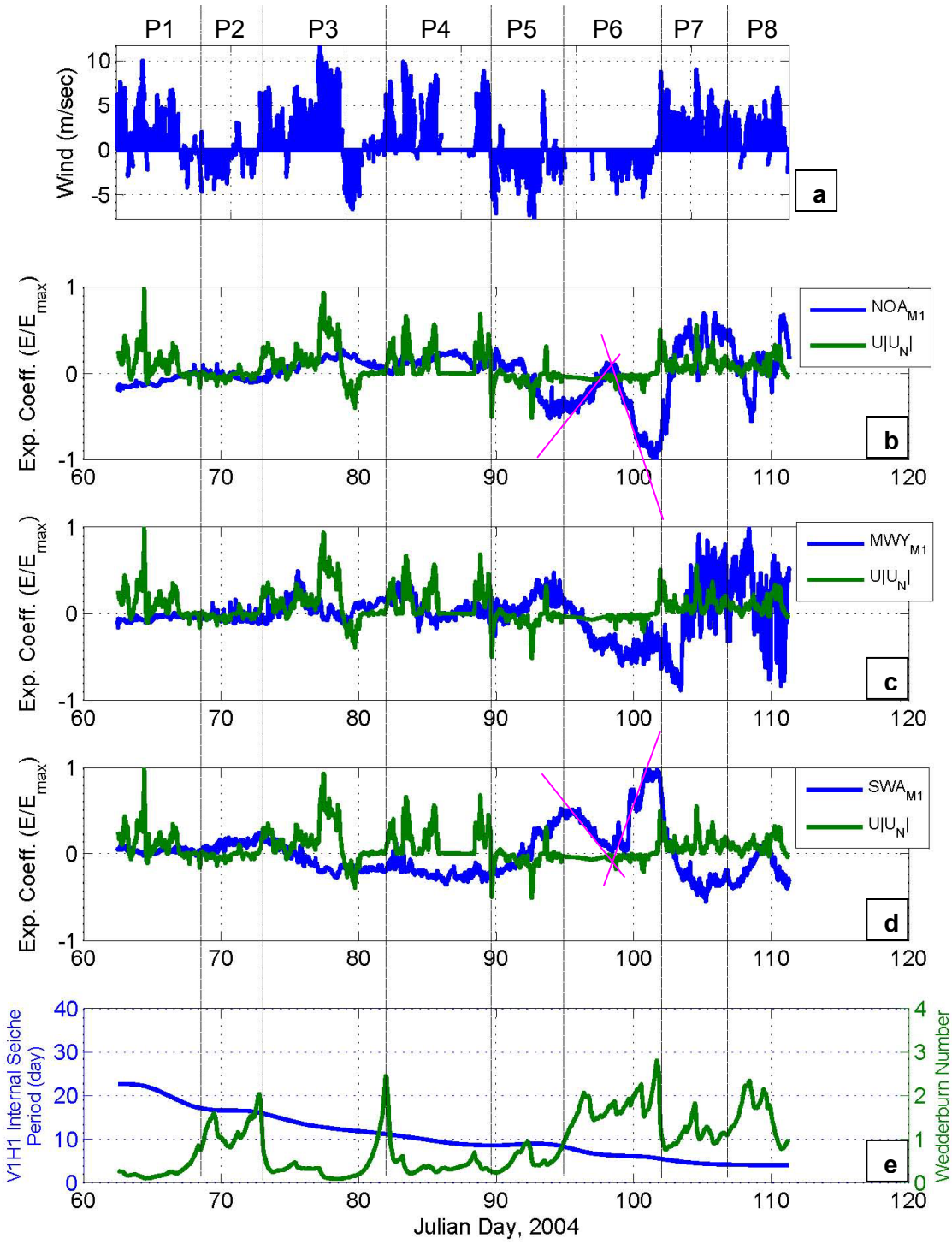


**Figure 1. 49.** Wind velocity vectors (a) and mode one expansion coefficients (blue lines) for NOA (b), MWY (c), and SWA (d); friction velocity is also shown (green line). Positive wind values mean it blows to the north. The Wedderburn Number (green line) and the period for a V1H1 internal seiche (blue line) are shown in (e). Red lines indicate instances when the wind stress shifted and complimented the density adjustment.

During P5 the wind stress shifted southward but still maintained $W_N$ below one; this change in direction enhanced the density adjustment. Before the wind shifted on JD 89.5, the thermocline had an upward north-to-south tilt (Figure 1. 38). After JD 90, the southward wind stress enhanced the internal seiche adjustment with significant down welling occurring near JD 95 at SWA and a corresponding upwelling occurred at NOA (Figure 1. 27). During the same time interval, the averaged densities reversed relative positions: SWA became lighter and NOA became denser (Figure 1. 23). The enhanced adjustment is determined by the amount of time it took the isotherm tilt to change direction. The 8.1 $^{o}$C isotherm dropped from 5 meters to 28 meters in about 2.2 days (Figure 1. 27). Based on linear theory, the tilt adjustment should take about four days (8/2) because the V1H1 internal seiche period was about eight days. At the end of P5 near JD 95, $W_N$ was near one and difference between the average density at NOA and SWA was largest (between JD 92 and 97, Figure 1. 23). This maximum difference indicated the maximum tilt occurred near JD 95.

At the start of P6 (JD 95), $W_N$ was near one, the wind stress was southward, and the isotherms were tilted upward from south to north (Figure 1. 49), but by JD 96.5 $W_N$ increased to 2 and the isotherm tilt had relaxed to a nearly neutral position (Figure 1. 40). Concurrently, the expansion coefficients increased (warmed) at SWA and decreased (cooled) at NOA, and the average density at SWA and NOA was nearly equal (Figure 1. 23 and Figure 1. 49). These results indicate the isotherms had adjusted to a nearly neutral position in 1.5 days, a little less than the 2 days linear theory suggests. Between JD 95 and 99.5, the wind direction is unknown but the wind speed could be estimated (§1.2.2); however, the upward north-to-south tilt and the enhanced adjustment time (1.5 verses 2) suggests a northward wind existed between JD 95 and 96.5. From JD 96.5 to JD 98.5 the isotherms adjusted past the neutral position to a slight upward tilt from north to south; the 9.3$^{o}$C isotherms is near 7 meters at SWA and 15 meters at NOA (Figure 1. 27). Between JD 99.5 and 103, significant down welling occurred at SWA with a corresponding upwelling at NOA (Figure 1. 27 and Figure 1. 42). During this time the wind was southward, which would have enhanced the adjustment from the upward north-to-south tilt on JD 98.5 to the upward south-to-north tilt on JD 102 (Figure 1. 27 and red lines in Figure 1. 49).

From P6 to P7 the wind shifted from southward to northward, $W_N$ decreased from 2.5 to less than one, and significant upwelling occurred at SWA with corresponding down welling at NOA (Figure 1. 27 and Figure 1. 42). During P7, $W_N$ generally remained near one and persistent tilt was observed with significant upwelling at SWA (Figure 1. 27 and Figure 1. 43). Additionally, the difference between the average densities at NOA and SWA were nearly the largest for the whole time series (Figure 1. 23). Near JD 104.5 $W_N$ increased for an interval less than a day and only a very minor adjustment was observed in the isotherms (Figure 1. 27). Based on linear theory, the time to adjust to the neutral position should be about 1.2 days (5/4), which is longer than the interval of the higher $W_N$.

During P8, $W_N$ increased from P7 and the isotherm tilt adjusted slightly. $W_N$ was about 2 between JD 108 and 110 when NOA isotherms moved higher in the water column and SWA moved lower in the water column (Figure 1. 27). Near JD 110, the wind stress increased, $W_N$ decreased to one, and the isotherms at SWA moved higher in the water column and lower in the water column at NOA (Figure 1. 27). During P8 an isotherm tilt was always present; the 10.5$^{o}$C isotherm was between 15 and 22 meters at NOA and always above 7 meters at SWA (Figure 1. 27).

For the 2004 observations, the baroclinic response was well described by the Wedderburn Number and the applied wind stress. The isotherms and average densities changed in the appropriate direction relative to changes in $W_N$; isotherm tilt relaxed when $W_N$ increased and tilt increased when $W_N$ decreased. Just as in the 2003 observations, baroclinic adjustments can be correctly inferred from relative changes in $W_N$. Based on the $W_N$ and wind stress analysis, the internal seiche behaved as a forced system; the persistent winds did not allow the internal seiche to freely oscillate. Because the relation between the isotherm tilt and $W_N$ was so good, $W_N$ should describe how much the isotherms deflect (1.8).

### 1.3.4 Application of Wedderburn Number to Isotherm Deflection

For the conceptual Wedderburn model, isotherm deflection is determined by the Wedderburn Number through (1.8) which specifies the interface deflection ($\zeta$) at the wall at the end of the lake and can be modified for an interior point ($L_{oc}$, (1.19)). If

the constant k is used as a regression coefficient, $W_N$ can be regressed against the observed isotherm deflections to obtain a relation that estimates isotherm deflection as a function of $W_N$ and location.

$$\zeta = h_1 + \frac{kh_1}{W_N}\left(\frac{2L_{loc}}{L}\right) \tag{1.19}$$

Where $\zeta$ is the interface deflection, L is the lake length (31 km), $h_1$ is depth to the density interface, k is a scaling constant, and $L_{loc}$ is the station distance from the center of the lake; specific values for $L_{loc}$ are given in Table 1. 11.

**Table 1. 11.** Station distances from the center of the lake. Based on SCAMP temperature contour plots, MWY station could be slightly north of center.

| Station | $L_{loc}$ (km) |
|---|---|
| NOA | 9.5 |
| MWY | 0.2 |
| SWA | 11.5 |

At the upwind end of the lake, (1.19) is positive for northward winds but the deflection should become negative for southward winds. To account for a changing wind direction, the tilt direction ($+W_N$ or $-W_N$ ) was determined from the sign of the expansion coefficients (Figure 1. 46 and Figure 1. 49). For example, for the 2004 NOA location an upward north-to-south tilt was defined by the positive expansion coefficient and an upward south-to-north tilt was defined by a negative the expansion coefficient. Isotherm deflections and $W_N$ values for the regression are given in Table 1. 12. Values for k are 0.27 for 2004 and 0.56 for 2003. For a purely two-layer lake, k=0.5; Stevens and Lawrence (1997) compared observed deflections for many lakes and plotted computed values of $W_N$ against measured $\zeta$ and $h_1$ for k=0.5 in (1.20). From their data, one can estimate a range of values for a fitted k, which ranged between 0.29 and 2.5.

$$W_N = \frac{kh_1}{\zeta} \tag{1.20}$$

The simple deflection equation and the Wedderburn Number provide a comparable dynamic response to the observed isotherms (Figure 1. 50 and Figure 1. 51). One should note that the superimposed deflection estimates the amplitude of the isotherm deflection; it does not represent the deflection of a particular isotherm. This condition is because, as the lake warmed, the particular isotherm that represented the density interface changed with time (Table 1. 12). At NOA from JD 61 to 90, SCAMP

isotherms typically showed a deflection greater than 25 meters, which agrees with the deflection computed with $W_N$ (Figure 1. 33 to Figure 1. 38 and Figure 1. 50). After JD 90, the model under-predicts the amplitudes but does quite well on the timing. Very similar responses are noted at SWA, but the timing of the deflection precedes isotherm response by about a day. The amplitude error could be from the simplistic use of a constant k; however, (1.19) captures the essences of the isotherm history and provides substantive evidence that lake dynamics are driven by wind.

**Table 1. 12.** Isotherm deflections and Wedderburn Number used for determining k in (1.19). The deflection was based on the depth of the noted isotherm at each location for the given Julian Day (JD).

| JD, Year | Isotherm ($^oC$) | Deflection (m) | | | | $W_N$ |
|---|---|---|---|---|---|---|
| | | SWA | MWY | NOA | NWA | |
| 61.5, 2004 | 7.26 | 10 | 28 | 42 | 35 | 0.434 |
| 68.5, 2004 | 7.58 | 4 | 5 | 17 | 23 | 0.751 |
| 75.5, 2004 | 7.48 | 8 | 25 | 35 | 35 | 0.396 |
| 89.5, 2004 | 8.14 | 8 | 14 | 35 | | 0.282 |
| 96.5, 2004 | 8.87 | 18 | 12 | 11 | 10 | 1.98 |
| 99.5, 2004 | 8.96 | 13 | 10 | 12 | 9 | 1.83 |
| 103.5, 2004 | 10.9 | 3 | 7 | 8 | 13 | 1.11 |
| 106.5, 2004 | 9.71 | 0 | 15 | 20 | 22 | 1.14 |
| 93.5, 2003 | 8.77 | 5 | 33 | 40 | | 0.459 |

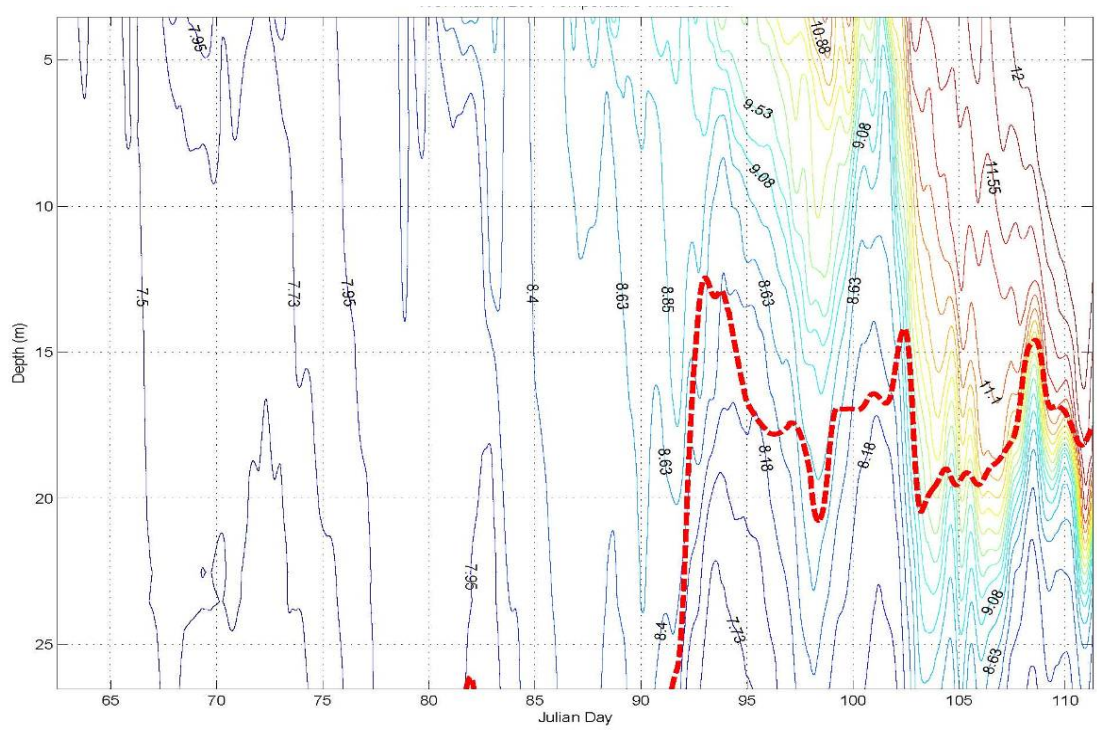


**Figure 1. 50.** NOA temperature time series for 2004 with calculated isotherm deflections (red-dashed line) using (1.19) for k=0.27. The red-dashed line estimates the deflection of the isotherms; it does not represent a particular isotherm.

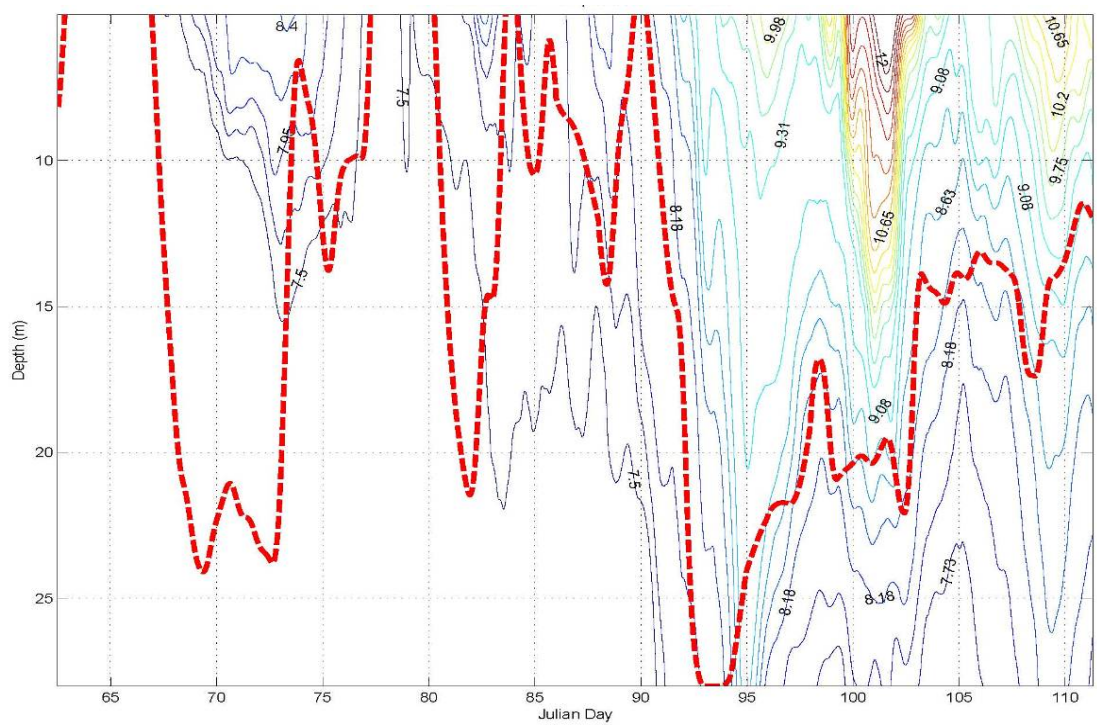


**Figure 1. 51.** SWA temperature time series for 2004 with calculated isotherm deflections (red-dashed line) using (1.19) for k=0.27. The red-dashed line estimates the deflection of the isotherms; it does not represent a particular isotherm.

### 1.3.5 Non-linear Wave Dynamics

The conceptual Wedderburn model assumed non-linear effects were negligible, but non-linear effects can produce significantly different behavior of the internal seiche. The Wedderburn Number describes the initial wave amplitude to the mixed-layer depth (1.19). The ratio of the wave amplitude to the water depth is a usual measure of the non-linearity of shallow-water waves; non-linear effects become important for $W_N \leq 1$, which occurred frequently in 2003 and 2004 observations. Non-linear waves have been observed along the density interface in long narrow lakes (Wiegand and Carmack, 1986; Farmer, 1977) and are likely to be common in small to medium-sized lakes subject to fairly uniform wind stress (Horn, Imberger and Ivey, 2001). The most important feature of non-linear waves is the rate of energy dissipation associated with non-linear waves versus linear; non-linear waves more rapidly dissipate large-scale internal waves compared to linear waves (Horn, Imberger, and Ivey, 2001). The non-linearity allows energy transfer from larger amplitude waves to smaller amplitude higher frequency waves (Hutter et al., 1998), which then break along the edges of the lake (Horn, Imberger, and Ivey, 2001; Boegman, Ivey, and Imberger, 2005). The periodicity of the larger wave is maintained and has nearly the same period as the linear wave, but its amplitude decays over time as energy is transferred to smaller waves; non-linear effects do not affect the initial set-up of the internal seiche (Hutter et al, 1998). The non-linear wave behavior is observed for freely developed gravity waves; however, in §1.3.2, §1.3.3, and §1.3.4 it was found that isotherm response was forced, and therefore non-linear wave characteristics should be minimal (as described above). If non-linear effects were present, the apparent affect would be a faster decay of the initial amplitude into smaller amplitude waves with higher frequency.

### 1.3.6 Modal Response for Depth Varying Buoyancy Frequency

The analyses have used a two-layer conceptual model for estimating the Wedderburn Number and internal seiche period (1.6) and (1.7), but the Wedderburn Number and period can be estimated for a linearly stratified system (1.11) and (1.12) . For a more general stratification, the internal wave phase speed can be obtained from the vertical temperature profiles for a non-rotating, stably stratified, Boussinesq fluid by solving the eigenvalue problem given by (Gill, 1982).

$$\frac{d^2w}{dz^2} + \frac{N^2 - \omega^2}{\omega^2} k^2 w = 0 \qquad (1.21)$$

Where N is the buoyancy frequency, w is the vertical velocity, ω is the frequency, and k is the horizontal wave number. Both w and N are functions of depth z.

The eigenvalue modal structures are determined by a thermal structure that is affected by wind, which can tilt the isotherms and change the vertical distribution of N from the static (no tilt) condition. Vertical density structure effects can be inferred from the two-layer internal seiche frequency,

$$\omega_n = \frac{2\pi}{T_n} = \frac{n\pi}{L}\left(\frac{g' h_1 h_2}{h_T}\right)^{1/2} \qquad (1.22)$$

Where $\omega_n$ is frequency for a given period $T_n$ and $h_T$ is $h_1$ plus $h_2$.
Errors in the upper layer depth $h_1$ are propagated into the frequency as shown by,

$$\Delta\omega = \frac{\omega}{h_1}\Delta h_1 \qquad (1.23)$$

Where $\Delta\omega$ is the frequency error as function of the upper layer error $\Delta h_1$; $\Delta$ is the change from the mean or non-tilted position. If $h_1$ is deflected upward then $\omega$ will increase and if $h_1$ is deflected downward then $\omega$ will decrease. One study found that the various modal response methods produced different values, which were different from the measured response. For Kootenay Lake, B.C., Canada, Wiegand and Carmack (1986) found a two-layer model estimated a mode one phase speed of 0.45 (m/s), the eigenvalue form was 0.35 (m/s), and the observed spectral response was 0.16 (m/s).

In 2003, V1H1 period was larger than the range in the eigenvalue periods (Table 1. 13). The eigenvectors also indicate the general location of the strongest thermal structure; on April 10, the mode one profiles indicate the thermocline tilts upward about 30 meters between the MWY and SEW locations, Figure 1. 52 and Figure 1. 53. The April 10 profile is presented because it was the only SCAMP profile taken within the RBR thermistor date range.

**Table 1. 13.** First mode periods estimated from the eigenvalue problem for the 2003 observations at four locations.

| Date | Eigenvalue | | | | V1H1 |
|---|---|---|---|---|---|
| | NOA | MWY | SEW | SWA | |
| April 10 (JD 99.5) | 5.4 | 4.8 | 6 | 5.1 | 7.9 |

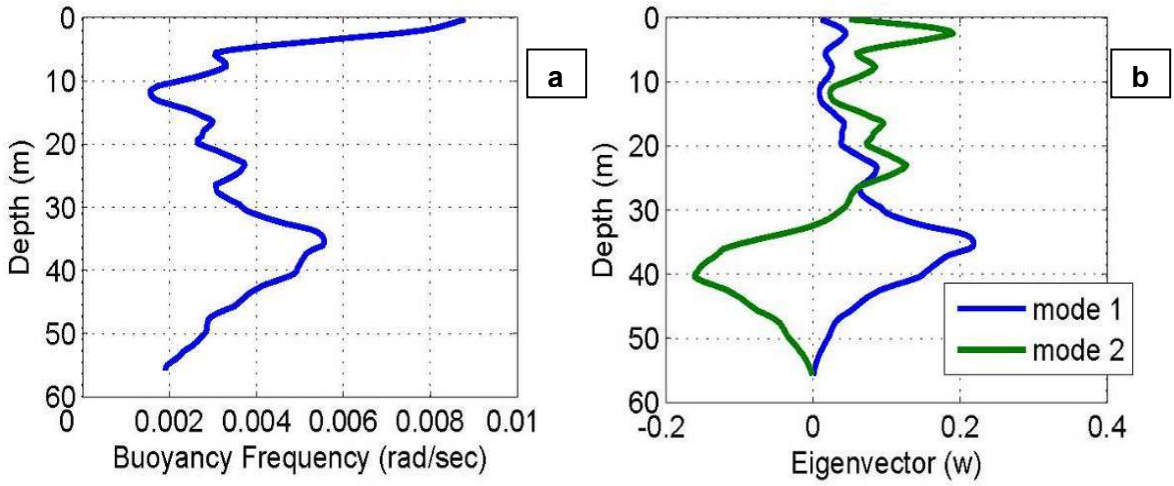


**Figure 1. 52.** Buoyancy frequency (a) and first and second modes for the normalized eigenvector for the vertical velocity profile (b) at MWY for April 10, 2003. The strongest thermal structure is located near the 35 meter depth. The unit rad is radians.

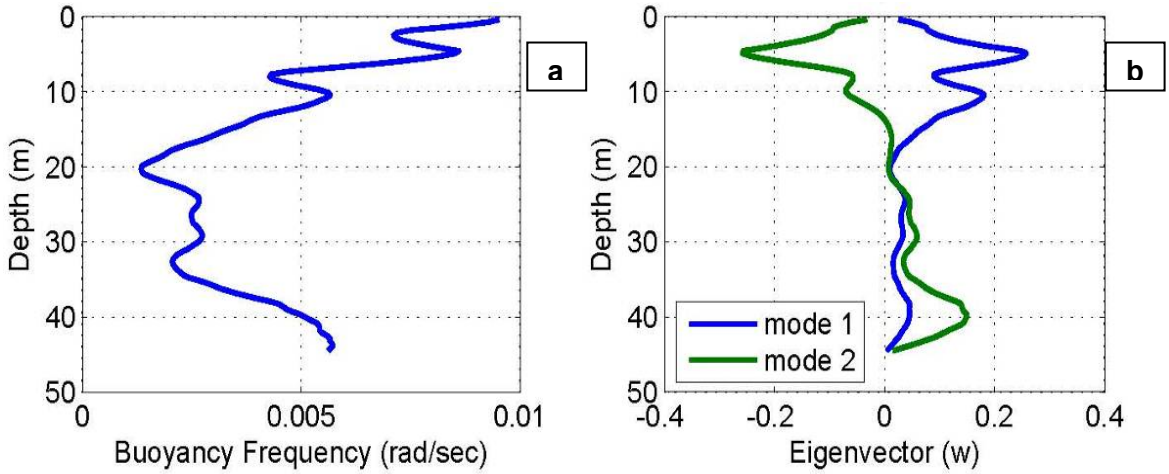


**Figure 1. 53.** Buoyancy frequency (a) and first and second modes for the normalized eigenvector for the vertical velocity profile (b) at SEW for April 10, 2003. The strongest thermal structure is located near the five meter depth. The unit rad is radians.

In 2004, temperature profiles show surface stratification in the upper five to 10 meters but the stratification was insufficient to suppress significant tilting of the isotherms (§1.3.2.2 and §1.3.3.3); however, it did define the eigenvalue modal features at the time of record and suggested the isotherm response should be limited

to the upper five to 10 meters (Figure 1. 54 and Figure 1. 55). The V1H1 periods were generally larger than first mode eigenvalue periods, but the range in eigenvalue periods were fairly large in March and to a lesser degree in April (Table 1. 14). The variation can be explained by the tilted isotherm structure. On March 16 (75.5), the isotherms tilted upwards from north to south and will produce a smaller frequency at NWA and a larger frequency at SWA (1.23). The period for the static condition should be between 16 and 5 days, the V1H1 period is between the two limits (14 (days), Table 1. 14).

**Table 1. 14.** First mode periods estimated from the eigenvalue problem for the 2004 observations at four locations.

| Date | Eigenvalues | | | | V1H1 |
|---|---|---|---|---|---|
| | NWA | NOA | MWY | SWA | |
| March 4 (68.5) | 10.10 | 8.68 | 9.49 | 6.22 | 17.1 |
| March 16 (75.5) | 16.34 | 7.29 | 4.98 | 5.77 | 13.8 |
| March 30 (89.5) | NA | 8.05 | 4.82 | 5.31 | 8.6 |
| April 6 (96.5) | 3.55 | 3.22 | 3.50 | 3.48 | 7 |
| April 9 (99.5) | 3.40 | 2.92 | 3.04 | 2.93 | 6 |
| April 13 (103.5) | 2.02 | 2.30 | 2.35 | 2.83 | 4.8 |
| April 16 (106.5) | 1.83 | 1.93 | 2.22 | 3.34 | 4.2 |

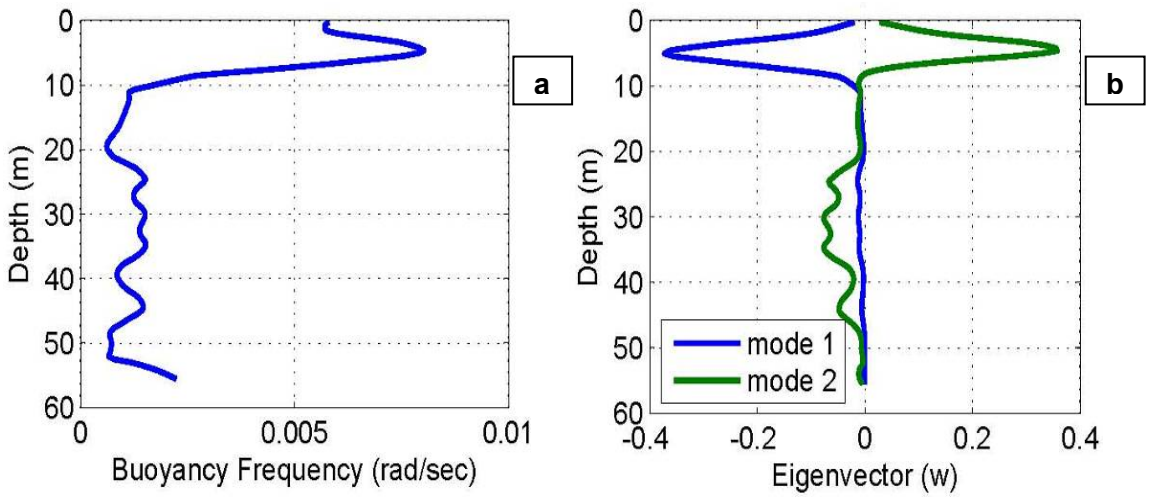


**Figure 1. 54.** Buoyancy frequency (a) and first and second modes for the normalized eigenvector for the vertical velocity profile (b) at MWY for March 9, 2004. March 9 is shown because it is near the start of the RBR thermistor date range. The unit rad is radians.

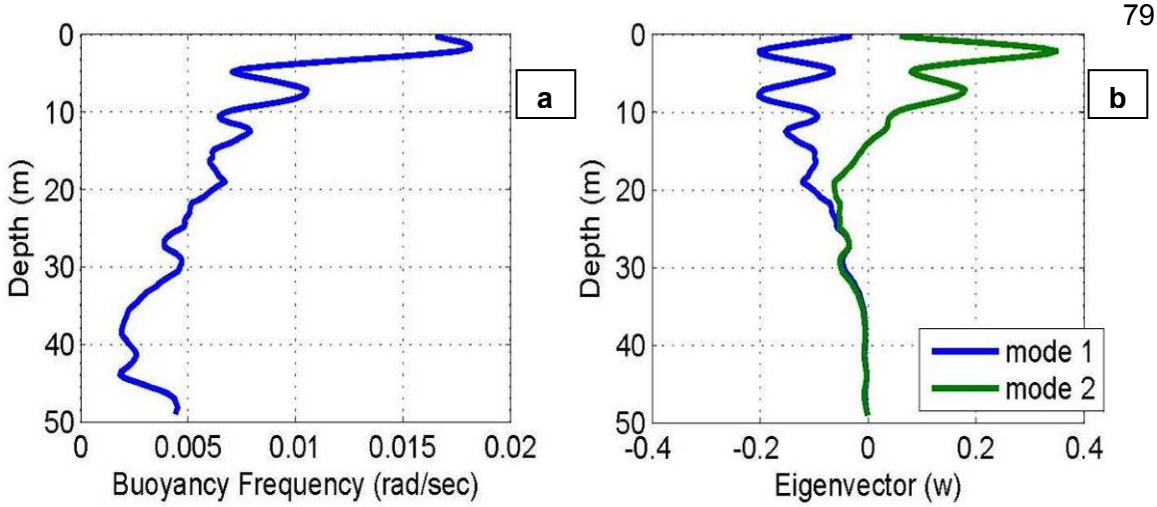


**Figure 1. 55.** Buoyancy frequency (a) and first and second modes for the normalized eigenvector for the vertical velocity profile (b) at MWY for April 6, 2004. April 6 is shown because it is near the end of the RBR thermistor date range. The unit rad is radians.

A Wedderburn Number based on linear stratification was not appropriate because none of the temperature profiles showed a linear decrease with depth; however, one can assess how different $W_N$ could be for typical buoyancy measured in the lake. The average buoyancy was about 0.008 (rad/sec) for April 6, 2004 and the average wind stress was about $2.5 \times 10^{-5}$ ($m^2/s^2$) for 2004. $W_N$ is about 0.01, which indicates that such a system would experience significant upwelling and tilting of the isotherms.

Based on the egienvalue solution, the estimated modal period is smaller than the period calculated for a two-layer V1H1 internal seiche; however, the eigenvalue solution is sensitive to the vertical temperature profile, which was shown to be affected by tilting of the isotherm. The April 2004 profiles indicated the maximum density interface occurred near the surface and that the internal seiche would have a more rapid and shallower response than the isotherm contours showed. The internal seiche probably had a period somewhere between the eigenvalue and two-layer solution and would not affect the results presented.

### 1.3.7 Effect of Cedar River on Temperature Observations at SWA

It has been shown that the observed isotherm response can be determined by the Wedderburn Number through the deflection equation (1.19), which functionally describes baroclinic effects from surface wind stress. However, potential influences

from the Cedar River have not been addressed; the observed isotherm oscillations or temperature record could be affected by inflowing water from the Cedar River. The Cedar River contributes approximately 57% of the hydraulic load where it discharges into the south end of Lake Washington. Previous analyses suggested that the river has some influence on nutrient concentrations at SWA (Arhonditsis, Brett, and Frodge, 2003). Thus, one might speculate that the river may also influence temperature at the south end, or that it could cause the observed deflections in the isotherms at SWA. In this section, evidence is presented that shows the Cedar has insignificant influence on average temperatures at SWA and does not cause the observed isotherm deflections.

1.3.7.1 Advective Diffusion Equation

To describe how the Cedar could affect isotherm oscillations, the Advective-Diffusion equation is used with the assumption that Cedar River water is cooler than the lake water; the cooler water flows underneath the warmer lake water This condition creates a two-layer system where the Cedar pushes the lake around from below, similar to conditions observed in salt-wedge estuaries. The interface and length of the intrusion is determined by vertical diffusion and horizontal velocity. Under steady-state, the vertical temperature profile is balanced by the longitudinal advection of temperature into the lake,

$$u\frac{\partial T}{\partial x} = D\frac{\partial^2 T}{\partial z^2}$$

Boundary and initial conditions

$$-D\ \frac{\partial T}{\partial z} + \alpha T = \alpha T_e; \quad z = 0 \qquad (1.24)$$

$$\frac{\partial T}{\partial z} = 0; \quad z = H$$

$$T(x,z) = T_0; \quad x = 0$$

Where u is the horizontal velocity, T is temperature, D is the vertical eddy diffusion, $T_e$ is an equilibrium temperature between the air and water surface, $\alpha$ is a heat flux coefficient, and $T_0$ is the temperature at the mouth of the Cedar River. The boundary condition at z=0 (1.24) allows the temperature flux to approach zero when heat input

is balanced by heat output. To solve (1.24), the non-homogenous boundary condition (BC) is transformed into a homogeneous BC using,

$$T(z,x) = T_e + \Upsilon(z,x) \tag{1.25}$$

Where T(z,x) is the sought solution and $\Upsilon(z,x)$ is the solution to the homogenous BC. Substituting (1.25) into (1.24) gives $\Upsilon(z,x)$ with homogenous BC,

$$u\frac{\partial \Upsilon}{\partial x} = D\frac{\partial^2 \Upsilon}{\partial z^2}$$

Boundary and initial conditions

$$-D\frac{\partial \Upsilon}{\partial z} + \alpha\Upsilon = 0; \quad z = 0 \tag{1.26}$$

$$\frac{\partial \Upsilon}{\partial z} = 0; \quad z = H$$

$$\Upsilon(x,z) = T_0 - T_e; \quad x = 0$$

Equation (1.26) has been solved by Carslaw and Jaeger (1959); solving for $\Upsilon(z,x)$ and substituting into (1.25) gives the solution,

$$T = T_e + 2\sum_{n=1}^{\infty} \frac{\lambda_n\left(T_0 - T_e\right)}{\left[\lambda_n^2 + \left(\frac{\alpha}{D}\right)^2\right]H + 2\frac{\alpha}{D}} \exp\left(\frac{-D\lambda_n^2 x}{u}\right) * A * B$$

$$A = \left[\cos(\lambda_n z) + \frac{\alpha}{\lambda_n D}\sin(\lambda_n z)\right] \tag{1.27}$$

$$B = \int_0^H \left(\lambda_n \cos(\lambda_n z) + \frac{\alpha}{D}\sin(\lambda_n z)\right) dz$$

$$\tan\left(\lambda_n H\right) = \frac{\alpha}{\lambda_n D}; \quad n = 1, 2, \ldots, \infty \tag{1.28}$$

Where x is horizontal distance, z is the vertical distance, and H is the water depth. The solution requires an infinite summation for the eigenvalues ($\lambda_n$) that solve the eigen-equations given by (1.28).

The purpose for solving (1.24) was to assess the longitudinal distance (x) that Cedar River flows could affect temperature conditions in Lake Washington; by inspection of (1.27), longitudinal variations are determined by a single term,

$$\exp\left(\frac{-D\lambda_n^2 x}{u}\right) \tag{1.29}$$

The source temperature $T_0$ decays exponentially with x distance (1.29) with the source temperature decaying by 1/e for $x = u/D\lambda_n^2$ ; $\lambda_n$ is a positive root that lies between (0,π)/H, (π,2π)/H… (Carslaw and Jaeger, 1959)). This relation implies Cedar River temperature effects effectively decay by 1/e for approximately $x = uH^2/D$ .

1.3.7.2 Conservation of Heat

If Cedar River discharge controls the temperature response at SWA over the depth of the thermistor array, then the temperature response at SWA should be a function of the heat flux from the Cedar. The temperature response will conform to a simple heat balance; the heat response at SWA should be a function of the heat input from the Cedar as,

$$\begin{aligned} H_{SWA}\left(Q_{Lake}+Q_{Cedar}\right) &= H_{Lake}\left(Q_{Lake}\right)+H_{Cedar}\left(Q_{Cedar}\right) \\ H_{SWA} &= \frac{H_{Lake}\left(Q_{Lake}\right)+H_{Cedar}\left(Q_{Cedar}\right)}{Q_{Lake}+Q_{Cedar}} \\ H_{SWA} &\approx H_{Cedar} \text{ for } \quad Q_{Cedar} >> Q_{Lake} \end{aligned} \tag{1.30}$$

Where Q is the flow from the lake or Cedar River and H is the heat from the lake, the Cedar River, and at SWA. From (1.30) one can write,

$$\left[c_p(T)\rho(T)T\right]_{SWA} \approx \left[c_p(T)\rho(T)T\right]_{Cedar} \tag{1.31}$$

Where $c_p$ is the specific heat, ρ is density, and T is temperature. Because all the variables are a function of temperature and for the heat at SWA to equal the heat at the Cedar River, the temperature at SWA must equal the temperature at the Cedar River.

$$T_{SWA} \approx T_{Cedar} \tag{1.32}$$

Equation (1.32) suggests the temperature at SWA should be highly correlated to Cedar River temperatures, if the Cedar River flows are much larger than lake circulation flows. Cedar flows and temperature were obtained from the USGS station 12119000 at 15-minute intervals; the average river flow was 26 m3/s in 2003 and 17 in 2004 (Table 1. 15). The SWA depth-averaged temperature time series was used for both years.

**Table 1. 15.** Flow statistics for the Cedar River for the study period in 2003 and 2004. The geometric mean flow (**μ**) and one-standard deviation (**σ**) are given.

| Year | Mean Flow (μ, $m^3/s$) | μ+σ ($m^3/s$) | μ-σ ($m^3/s$) |
|---|---|---|---|
| 2003 | 26.4 | 37.3 | 18.7 |
| 2004 | 16.6 | 21.1 | 12.9 |

Before the temperature time series were analyzed, the temperature time series were standardized as suggested by Hann (1997),

$$X_{ij} = \frac{x_{ij} - \bar{x}_j}{s_j} \tag{1.33}$$

Where $X_{ij}$ is the standardized variable, $x_{ij}$ is the observed variable, $x_j$ (super bar) is the mean of $x_{ij}$, and $s_j$ is the variance of $x_{ij}$. The variables were detrended from a fitted curve.

1.3.7.3 Flow, Momentum, and Buoyancy Dimensional Analyses

At the south end of the lake, the Cedar River will control hydrodynamics under sufficient flow and momentum; the length of the lake controlled by the Cedar River plume can be determined by dimensional analysis. The length scale in which flow dominates ($l_Q$) is determined by the width of the river; the length scale in which momentum dominates ($l_M$) is determined by the momentum and buoyancy ((1.34), Fischer et al., 1979). At lengths greater than $l_M$, plume dynamics are largely controlled by buoyant forces.

$$l_Q = W$$
$$l_M = \frac{M}{B^{2/3}} \tag{1.34}$$

Where W is the channel (slot) width, M is momentum per unit length of channel, and B is buoyancy per unit length of channel (Fischer et al., 1979); $l_Q$ and $l_M$ provide an order of magnitude estimate of the distance that the Cedar River flow or momentum

could significantly affect hydrodynamics in the lake. At lengths greater than $l_M$, the river plume would passively affect dynamics in the lake because of buoyancy differences between the river plume and the lake.

1.3.7.4 2003 and 2004 Temperature Observations

Correlation analysis indicated Cedar River temperature explained very little of the observed temperature response at SWA. For the April 2003 observations, the depth-averaged temperature time series at SWA was positively correlated to the Cedar River temperature (Figure 1. 56); the correlation coefficient was 0.14, which suggests about 2% of the observed temperature variance at SWA was explained by temperatures from the Cedar River (Table 1. 16). In March 2004 SWA temperatures were positively correlated with the Cedar temperature and the correlation was larger than in 2003 (R=0.2), but again the Cedar River had very little influence ($R^2$=4%) on the depth-averaged SWA temperature time series at SWA (Table 1. 16 and Figure 1. 57). The Cedar temperature had a significant diurnal signal, which was not present at SWA to any significant degree (Figure 1. 56 and Figure 1. 57). Diurnal fluctuations can be removed by applying a 24-hour moving average (MA) filter to the series. Correlations between the 24-hour MA did not show substantially different linear relations; the March 2004 correlation increased to 4% from 8% (Table 1. 16). This analysis suggests the Cedar River flows were not sufficient to affect temperature conditions at SWA; temperature flux from the Cedar River was dampened by wind-generated flows in the lake.

**Table 1. 16.** Correlation coefficient and P-values between the standardized observations at SWA and the Cedar River; the correlation was between the averaged temperature time series and Cedar River temperature series. Statistics for the observed series and the 24 hour moving average (MA) are presented.

| Year | Data type | Correlation coefficient (R) | $R^2$ | P-value |
|---|---|---|---|---|
| April 2003 | Observed | 0.14 | 0.02 | 0.000 |
| | 24 hour MA | 0.13 | 0.02 | 0.000 |
| March 2004 | Observed | 0.20 | 0.04 | 0.000 |
| | 24 hour MA | 0.29 | 0.08 | 0.000 |

During upwelling conditions at the south end of the lake, wind generated flows in the lake significantly dampened temperature fluxes from the Cedar River. In 2003 between Julian Day 91 - 112, the depth and time average horizontal velocity below the SR520 bridge was 1.14 (cm/s) from 3 to 11 meters and at MWY it was 0.14

(cm/s) from 8 to 20 meters (Table 1. 17). Substituting the average Cedar River flow (26 ($m^3$/s)) and potential wind-driven flow (342 ($m^3$/s)) into (1.30), the Cedar would have about a 7% to 8% effect on temperature at SWA (Table 1. 17).

**Table 1. 17.** Potential wind-driven flows for depth and time-averaged velocities obtained at SR520 and MWY during the 2003 field program. For windy events during years 2003 and 2004, the larger wind events obtained wind speeds of approximately 8 (m/s). A Cedar River flow ($Q_{Cedar}$) of 26 ($m^3$/s) is used to determine the temperature effect from the Cedar River at SWA.

| Velocity (cm/s) | Typical Depth of Flow (m) | Flow for a Width of 3 km. ($Q_{Lake}$, $m^3$/s) | $\frac{Q_{Cedar}}{Q_{SWA}+Q_{Cedar}}$ |
|---|---|---|---|
| 1.14 | 10 | 342 | 7% |
| .47(1) | 20 | 324 | 8% |
| 24(2) | 5 | 3600 | 0.7% |
| (1) 0-20 meter depth average of the SR520 and MWY<br>(2) 3% of a 8 (m/s) wind | | | |

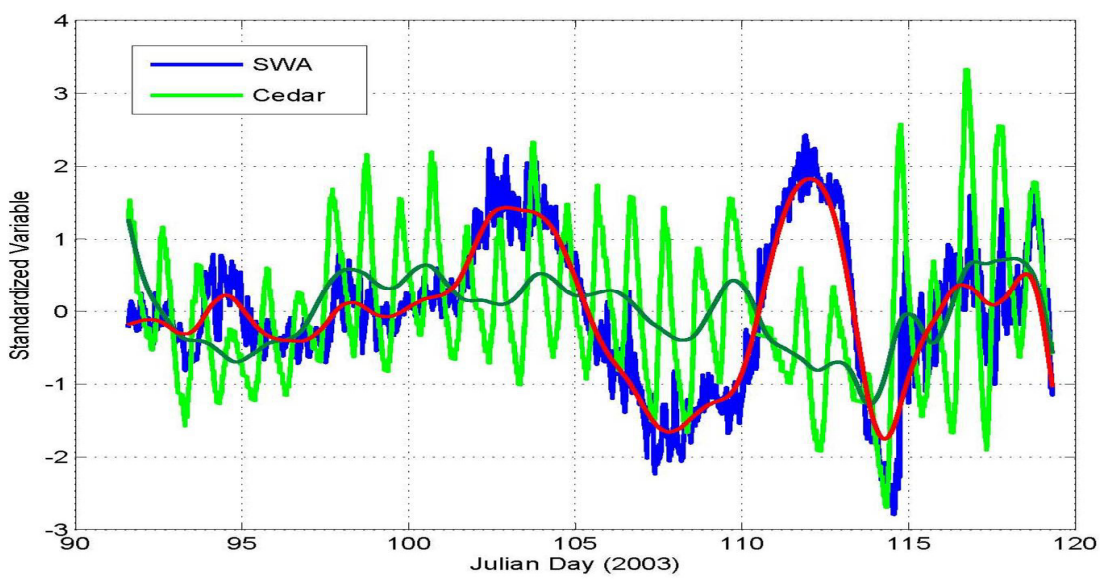


**Figure 1. 56.** Standardized observations for the averaged temperature at SWA (blue) and Cedar River Temperature (green) for April 2003. The red line is the 24 hour moving averaged for SWA and the dark green line is the 24 hour moving average for the Cedar.

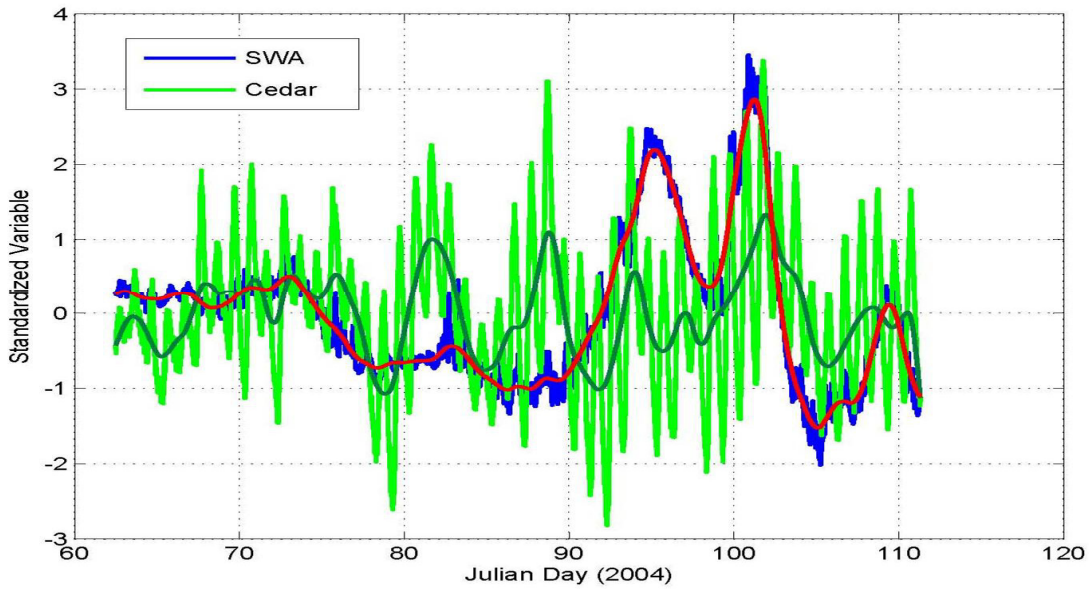


**Figure 1. 57.** Standardized observations for the averaged temperature at SWA (blue) and Cedar River Temperature (green) for March 2004. The red line is the 24 hour moving averaged for SWA and the dark green line is the 24 hour moving average for the Cedar.

1.3.7.5 Flow, Momentum, and Buoyancy

The temperature correlation suggested Cedar River flows were insignificant to affect temperature observations at SWA; dimensional analyses also indicated the Cedar River had insufficient momentum to affect hydrodynamic conditions at the south end of the lake. The Cedar River had insufficient momentum to affect hydrodynamics beyond about 200 meters from the mouth (Table 1. 18). The analysis assumed a mean flow plus one standard deviation (Table 1. 15), a river depth of 1.5 meters and width of 40 meters, which was determined from King County aerial orthographic photos.

**Table 1. 18.** Momentum length scale ($l_M$) for average temperatures in the Cedar River ($T_{Cedar}$) and Lake Washington at SWA ($T_{SWA}$). Flows from the Cedar River ($Q_{Cedar}$) represent the mean plus one standard deviation (Table 1. 15) and momentum ($M_{Cedar}$) and buoyancy ($B_{Cedar}$) terms are per unit width of the river.

| Year | $T_{SWA}$ (°C) | $T_{Cedar}$ (°C) | $Q_{Cedar}$ ($m^3/s$) | $U_{Cedar}$ (m/s) | $M_{Cedar}$ ($m^3/s^2$) | $B_{Cedar}$ ($m^3/s^3$) | $l_M$ (m) |
|---|---|---|---|---|---|---|---|
| 2003 | 8.82 | 9.06 | 37 | 0.62 | 0.57 | 1.54E-04 | 199 |
| 2004 | 7.98 | 9.2 | 21 | 0.35 | 0.18 | 4.33E-04 | 32 |

1.3.7.6 Advective-Diffusion of Temperature

The Advective-Diffusive equation solution shows the longitudinal influence of the Cedar River has exponential form and that the length is dependent on river velocity,